Generation of a selected Lamb mode by piezoceramic transducers : application to nondestructive testing of aeronautical structures

Farouk Benmeddour, Emmanuel Moulin, Jamal Assaad, S. Djili

Chapter 5

Generation of a Selected Lamb Mode by Piezoceramic Transducers: Application to Nondestructive Testing of Aeronautical Structures

Farouk Benmeddour, Emmanuel Moulin,
Jamal Assaad and Sonia Djili

Additional information is available at the end of the chapter

http://dx.doi.org/10.5772/54582

1. Introduction

The motivation of the this work is highlighted by the need for the Non-Destructive Testing (NDT) of aircraft, petrochemical and naval structures. Functioning conditions of these structures and the time factor can lead to serious damage. The most appropriate NDT technique to plate-like structures seems to be guided ultrasonics Lamb waves [1]. These waves can carry out energy over long distances and have the potential to be sensitive to several types of defects. Consequently, their use allows fast and efficient inspections of industrial structures. However, the multimode and dispersive nature of Lamb modes make the interpretation of the received ultrasonic signals complex and ambiguous in presence of discontinuities. Moreover, the generation and reception of a selected Lamb mode by transducers remains a difficult task due to the complexity of guided waves.

In this work, two identical thin piezoceramic transducers are designed specifically to work in the frequency band of interest. The generation of a specific Lamb mode is ensured by the placement of these transducers at the opposite sides of the plate. The selection of the A_0 or the S_0 mode is obtained by exciting the piezoceramic transducers with in-anti-phased or in-phased signal, respectively. Then, interactions of these modes with discontinuities in aluminium plates are investigated. The interaction of Lamb waves with discontinuities has been widely analysed. Among the studied defects, one can cite holes [2], delaminations [3], vertical cracks [4], inclined cracks [5], surface defects [6], joints [7], thickness variations [8] and periodic grating [9]. Moreover, the special case of rectangular notches have been carried out by Alleyne et al [10], Lowe et al [11], Jin et al [12] and Benmeddour et al [13–15].

The Two-Dimensional Fourier Transform (2D-FT) is commonly used by researchers [3, 15, 16] to identify and quantify the existent Lamb modes. However, this technique needs spatio-temporal

sampling which is time consuming and not always available from experimental measurements. In this paper, the scattered waves are acquired by means of conventional piezoelectric transducers located on the plate surfaces in front and behind the damage. The fundamental Lamb modes are separated by means of the basic arithmetic operations such as addition and subtraction. This approach allows a simple separation by using only two signals acquired at the same location on the opposite sides of the structure. Hence, the reflection and the transmission of the incident and the converted fundamental Lamb modes, when they exist, can be identified and quantified. The power reflection and transmission coefficients are then obtained with the well-known average power flow equation and the power balance is verified. Measurement results confirmed that symmetric discontinuities could not induce any mode conversion in the contrary of asymmetric discontinuities. The sensitivity of the A_0 and S_0 mode is checked.

An approximation technique of the reflection and transmission of the fundamental Lamb waves from rectangular notches is used. This technique is based on the superposition of the reflection and the transmission from a step down (start of the notch) and a step up (end of the notch). To this end, an approach based on the power reflection and transmission coefficients is proposed. These power coefficients take into account only a single echo and only the A_0 and S_0 modes are studied at a given frequency taken under the cut-off frequency of the A_1 and S_1 modes, respectively. The power coefficients are determined with the help of the finite element and the modal decomposition method. The Finite Element Method (FEM) is used to compute the displacement fields, while the modal decomposition method allows to calculate the power coefficients from these displacements at a given location on the plate surfaces. Then, this aims to compute the power reflection and transmission coefficients for a notch from those obtained for a step down and a step up. The advantages of such a study are that the power coefficients of the multiple reflections can be determined even if the structure contains different thickness variations. Moreover, it allows the study of the interaction of the fundamental Lamb waves with complex discontinuities in a fast and efficient way.

Finally, experimental measurements are compared successfully with those obtained by the numerical method.

2. The piezoelectric transducers

2.1. Applications of the piezoelectric transducers

Since several decades, piezoelectric transducers are widely used in many fields of application. Some of these fields are reported hereafter. Si-Chaib et al[17] have generated shear waves by mode conversion of a longitudinal wave by using straight ultrasonic probes coupled to acoustic delay lines. The device is used in the field of mechanical behaviour of materials and the determination of acoustic properties of porous materials. Duquennoy[18] et al have used both laser line source and piezoelectric transducers to characterise residual stresses in steel rods. They measured the velocities of Rayleigh waves. Yan et al[19] have developed a self-calibrating piezoelectric transducer for the acoustic emission application. Blomme et al[20] have designed a measurement system with air-coupled piezo-based transducers. Their work deals with coating on textile, flaws in an aluminium plate, spot welds on metallic plates, tiny air inclusion in thin castings and ultrasonic reflection on an epoxy plate with a copper layer. Martínez et al[21] have designed a prototype of segmented annular arrays to produce volumetric imaging for NDT applications. Bhalla and Soh[22] have used high frequency piezoelectric transducers to monitor reinforced concrete subjected to vibrations caused by earthquakes and underground blasts. Sun et al[23] have bounded piezoceramic patches on concrete beams to investigate the structural health monitoring.

http://dx.doi.org/10.5772/54582

Rathod and Mahapatra[24] have chosen a circular array of piezoelectric wafer active sensors (PWASs) to localise and identify corrosion in metallic plates. The study is based on the guided Lamb waves and an algorithm based on symmetry breaking in the signal pattern.

Other types of transducers have been also developed and studied in the literature for several applications. A brief discussion about only some types of transducers is given here. Chung and Lee [25] have fabricated focusing ultrasound transducers based on spin-coated poly(vinylidene fluoride-trifluoroethylene) copolymer films. These films can be used for high frequency wave velocity measurements and for nondestructive determination of elastic constants of thin isotropic plates. Ribichini et al [26] have used electromagnetic acoustic transducers (EMATs) for their experimental measurements on different types of steel. They show the performance of bulk shear wave generated by EMATs to investigate the physical properties of materials. Lee and Lin [27] have fabricated a miniature-conical transducer for acoustic emission measurements. Bowen et al[28] have fabricated flexible ultrasonic transducers and tested a steel rod in pulse-echo mode.

2.2. Design and characterisation

Two piezo-ceramique transducers are cut in a plate of 50×50 mm^2 with the following dimensions. The length of these transducers is chosen to be $L = 50$ mm to be able to generate a unidirectional wave. The width of $w = 6$ mm corresponds to the half of the wavelength of the A_0 mode at the chosen working frequency of 200 kHz. The thickness of the transducers is equal to 1 mm. Figure 1, depicts the dimensions of a piezo-ceramic transducer used in this work. These transducers are handled by the company Ferroperm and the used piezo-ceramic type is a soft lead zirconate titanate Pz27. This material presents a high electromechanical coupling coefficients. The mechanical characteristics of the Pz27 given by the constructor are: a density of $\rho = 7700 kg/m^3$, the elastic compliances $s_{11}^E = 17 \times 10^{-12} m^2/N$, $s_{11}^D = 15 \times 10^{-12} m^2/N$, the Poisson's ratio $\nu^E = 0.39$ and the mechanical quality factor $Q_m = 80$; here, the superscripts E and D designate electrical short and open circuits, respectively. Some of the piezoelectric constants are: the coupling factor $k_{31} = 0.33$, the piezoelectric charge coefficient $d_{31} = -170 \times 10^-12 C/N$ and the piezoelectric voltage coefficient $g_{31} = -11 \times 10^{-3} Vm/N$.

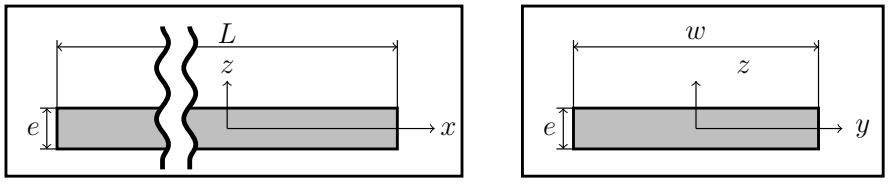

(a) (b)

Figure 1. The geometry and dimensions of the piezo-ceramic transducers (a) front view and (b) side view (arbitrary scale).

The two piezo-ceramic transducers are then characterised by a network analyser. The electrical phase and normalised module impedance are shown in figures 2a and b, respectively. It is observed that the curves of the two transducers are close each other. In addition, this can confirm the working frequency of 200 kHz and the working region near to the resonance frequency

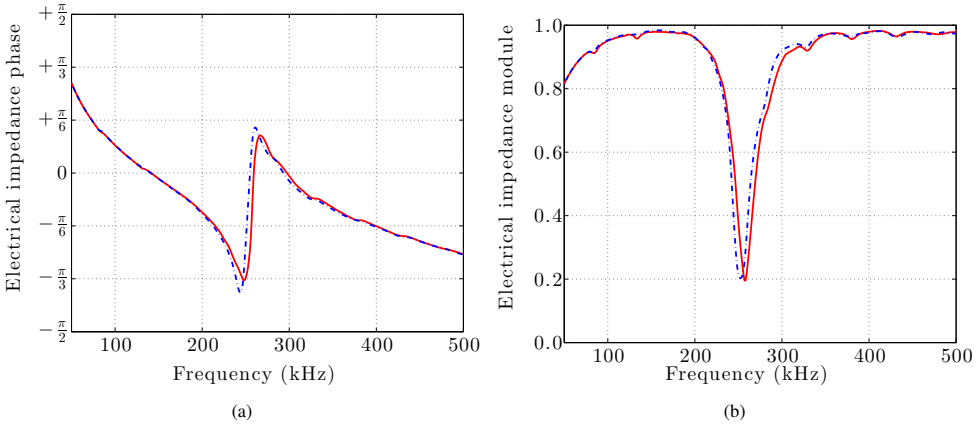

Figure 2. Electrical impedance of (a) phase and (b) module of the two used transducers (—) transducer 1 and (—·) transducer 2.

The receiver, in this work, is an industrial transducer designed by Olympus. It is a Panametrics type with the reference A413S. Its working center frequency is 500 kHz and have a good sensitivity. The nominal element size have the dimensions of 13×25 mm^2. This transducer is also used as an emitter to characterise the aluminium plate and will be explained hereafter.

2.3. The emitter

This work aims to generate a selected guided wave in an aluminium plate. To this end, the two piezoceramic transducers are placed on the two faces of the plate in opposite position (see figure 3). It was shown [15] that the excitation of transducers with anti-phased electrical signals generates favouringly an anti-symmetrical guided wave. The excitations of these transducers with in-phased electrical signals however, produces mainly a symmetrical guided wave. The excitation of transducers is ensured by two function generators and synchronised by a pulse generator.

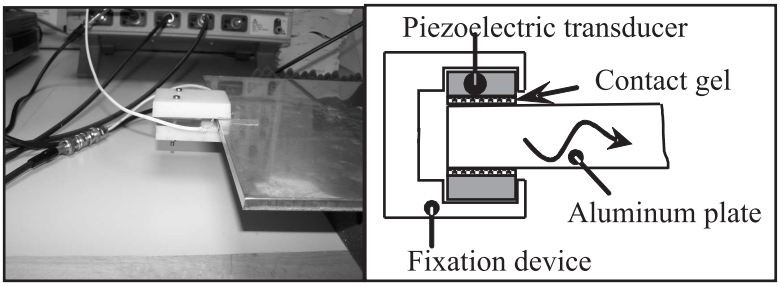

Figure 3. A photo of the piezoceramic support in-site (left) and a front view of its schematic description (right).

http://dx.doi.org/10.5772/54582

3. The experimental device

3.1. General description

As described briefly in the last section, a pulse generator (HM 8035) is used to trigger simultaneously the two arbitrary function generators (HP 33120A) and the oscilloscope (Le Croy type LT344). The function generators are able to generate a tone burst electrical signals windowed by a Hanning function to the emitter. Each of the in-phased or anti-phased signals are made of 5 sinusoidal cycles at the frequency of 200 kHz windowed by a Hanning function. The oscilloscope acquires 2000 temporal points at a sampling frequency of 10 MHz which corresponds to 0.1 μs between each point and verify the Shannon sampling theorem. Fifty acquired signals are averaged by the oscilloscope with an error less than 0.5%. Then, the result is transmitted to the computer for recording and signal processing. Furthermore, the repeatability process and the gel coupling effect are studied. To this end, the receiver is removed and replaced at the same location 20 times. Hence, an error bar can be computed for each experience.

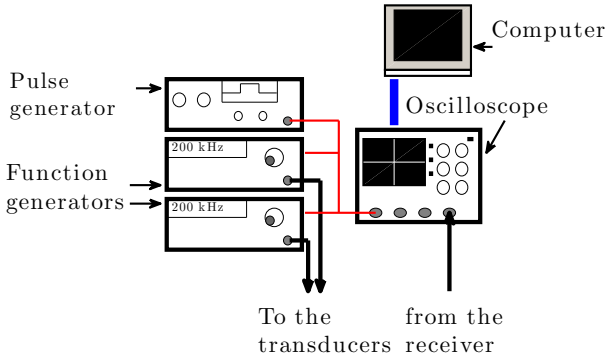

Figure 4. The scheme of the experimental device.

In what follows, aluminium plates are experimentally investigated. They have the following dimensions: 6 mm thick, 300 mm wide and 500 mm long.

3.2. Material characterisation

Before starting with experimental measurements which aim to select and generate one Lamb mode, one must characterise the plate material. For this purpose, the Panametrics transducer is used to generate a one pulse signal at a frequency of 500 kHz. Then, with a second Panametrics transducer, 256 signals are squired on a line on the surface of the plate with a 1 mm of distance between two positions. The application of a two dimensional fast Fourier transform gives rise to the dispersion curves. Figure 5, represents these dispersion curves in addition of the theoretical results computed for an aluminium plate with the following characteristics: the density $\rho = 2695$ kg·m^3, the Young's modulus $E = 72.10$ GPa and the Poisson's coefficient $\nu = 0.383$. In this figure, it is clearly shown that the chosen parameters correspond to the characteristics of the used aluminium plate. This has the advantage to identify Lamb modes by their group velocities.

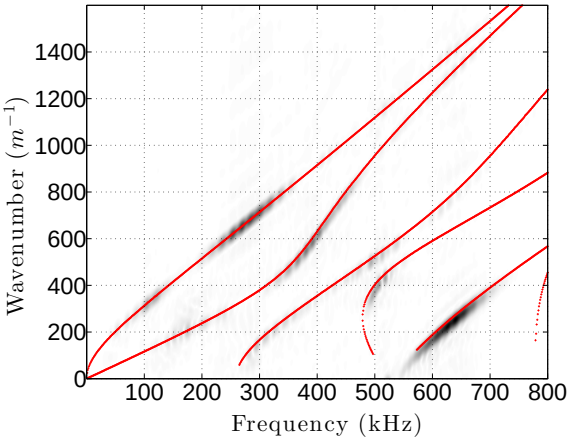

Figure 5. Experimental and analytical dispersion curves of wavenumbers vs. frequency.

3.3. Experimental measurements

By using the experimental device described and shown on figures 3 and 4, experimental measurements are carried out for in- and anti-phased electrical signals. These results are shown on figures 6a and b where the Panametrics receiver is placed at a distance of $l_1 = 185$ mm from the left edge of a healthy plate (115 mm from the right edge). The time of flight (TOF) is used to determine the group velocity of each wave packet. In fact, the used TOF is taken as the peak of the signal envelope (by using the Hilbert function) which corresponds to the center working frequency. Wave packets are clearly identified by their group velocities as the first antisymmetric (A_0) and the first symmetric (S_0) Lamb modes, respectively. In both cases, the selection of one Lamb mode is successful, which validates the experimental set-up. Since the S_0 mode has a higher group velocity than the A_0 mode, its reflection on the right edge of the plate is visible.

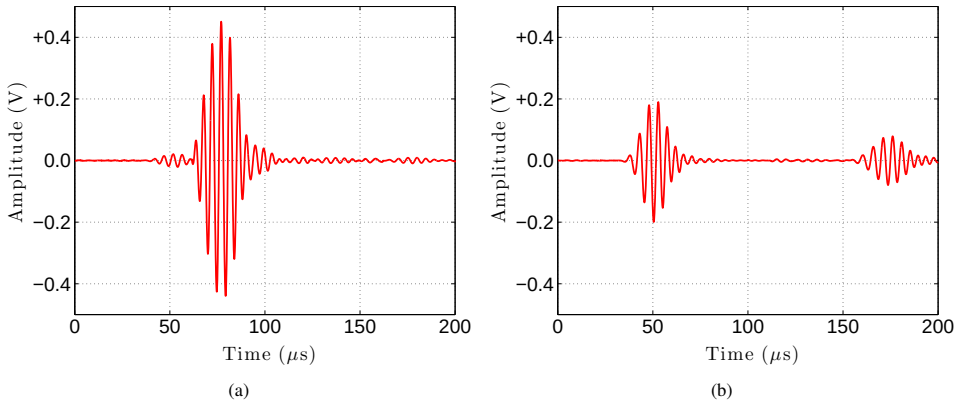

Figure 6. Measured signals when transducers are excited with (a) in-phased and (b) anti-phased electrical signals.

http://dx.doi.org/10.5772/54582

4. Application to the damage detection

4.1. Experimental measurements

The experimental measurements investigate the interaction of the fundamental Lamb modes A_0 and S_0 with two discontinuity kinds: symmetric and asymmetric shape-like notches. These notches are milled across the full plate width (300 mm) normal to the transmission path and have a width of 50 mm. Six notch depths are experimented and are equal to: 0.5, 1, 1.5, 2 and 2.5 mm which corresponds to the ratios p=5/6, 4/6, 3/6, 2/6 and 1/6, respectively. The desired notches width and depths are obtained with a conventional milling machine.

Owing to the existence of two modes, additional measurements and operations are conducted to separate them. To do so, signals are acquired on the two faces of the plate at exactly the same location. Then, the basic addition and subtraction operations are used. The former aims to amplify the antisymmetric mode and attenuate the symmetrical one. The latter however gives rise to enhance the symmetrical mode and to disfavour the antisymmetrical mode.

4.1.1. Calibration handling

Experimental measurements are carried out to study the receiver presence effect on the transmitted wave packets. Therefore, an identical Panametrics receiver is placed between the emitter and the conventional effective receiver. Hence, the measured signals when the A_0 and S_0 modes are launched, respectively are disturbed. In fact, the presence of the conventional transducer along the propagation path can be considered as a surface perturbation because of its dimensions ($39\times17\times15$ mm^3). Hence, the amplitude of the A_0 mode decreases to about 40%. Furthermore, its shape is modified by the multiple reflections from the edges of the receiver. Contrarily to this, the S_0 mode decreases only to about 5%.

In practice, when a fundamental Lamb mode is launched at the left edge of the plate, the incident wave packet encounter the conventional receiver. Then, the disturbed transmitted wave packet is reflected by the left edge of the discontinuity and then received. Hence, the measured reflection wave packet must be corrected by multiplying its amplitude by 40% when the A_0 mode is launched whereas the amplitude of the reflection wave packet is multiplied by only 5% when the S_0 mode is launched.

For the transmitted wave packet after the discontinuity, the transmitted amplitude does not need any correction. However, in order to take into account implicitly the dispersion, the diffraction and the attenuation effects, the incident wave packet is acquired on a healthy plate at the same location as the transmitted wave packet in a damaged plate.

4.1.2. Symmetrical notches

Figures 7a and 7b display the addition and the subtraction mean results, respectively of the electrical signals measured before a symmetrical notch when the A_0 mode is launched for a plate containing a 2.5 mm deep notch (p=1/6 of normalised thickness of the plate). By means of the flight time and the shape observation of each wave packet, no mode conversion from the incident A_0 to the S_0 mode is observed in the figure 7a. On this figure, the first and the second wave packets correspond to the incident (in) and the reflection (re_1) from the first edge of the notch. Furthermore, multiple reflections from the edges of the notch and the plate are observed. Figure 7b proves one more again that no significant mode conversion is noticed and the observed small wave packets rises mainly from the emitter.

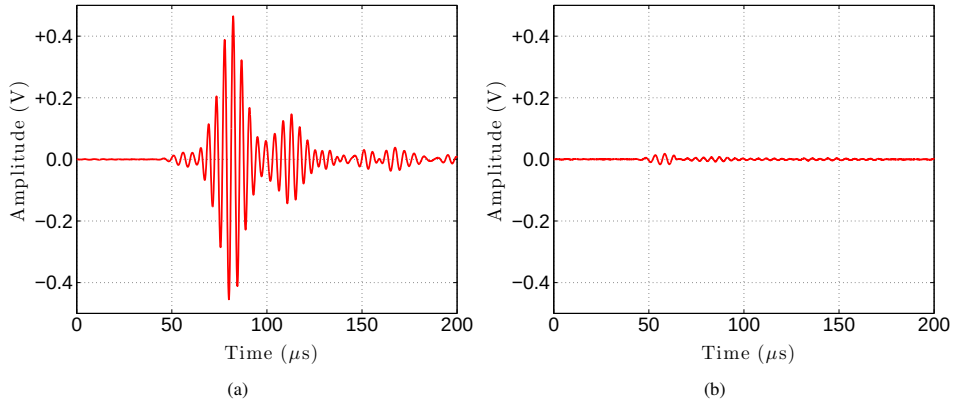

Figure 7. (a) addition and (b) subtraction mean results of the electrical signals measured before a symmetrical notch of 2.5 mm of deep (p=1/6) when the A_0 mode is launched.

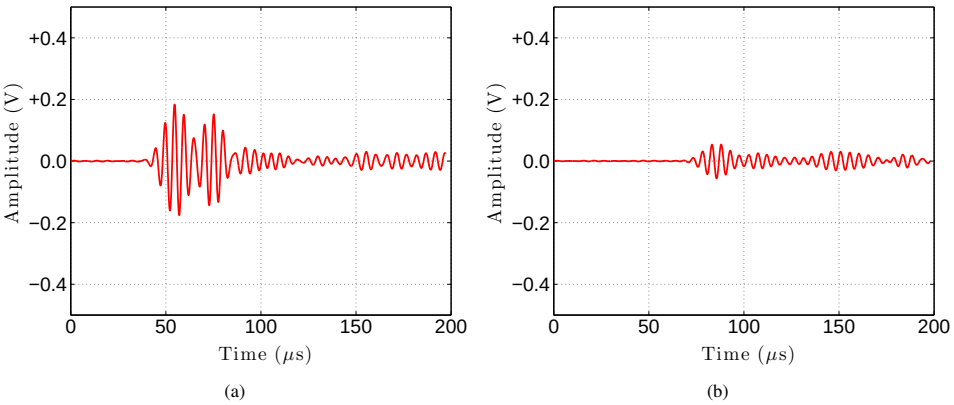

Figure 8. Subtraction mean results (a) before the notch at 185 mm and (b) after the notch at 315 mm from the left plate edge.

Figures 8a and b depict only subtraction mean results of the electrical signals measured before (185 mm from the left edge) and after (315 mm from the left edge) a symmetrical notch, respectively when the S_0 mode is launched for a plate containing a 2.5 mm deep notch (p=1/6).

In figure 8a the first and the second wave packets correspond to the incident (in) and the first reflection (re_1) from the left notch edge of the S_0 mode. Furthermore, multiple reflections from the notch and plate edges are observed. Figure 8b display the second transmission (tr_2) after the notch of the S_0 mode. Here again, no mode conversion is observed and the addition mean results are not shown for brevity and conciseness.

Since each wave packet is identified and quantified, the Hilbert transform is used to evaluate the wave packets' peaks. These measurements are used to compute the power flux energy which are shown hereafter.

http://dx.doi.org/10.5772/54582

4.1.3. Asymmetrical notches

Figures 9a, b, c and d display the mean results of addition (Figs. 9a and d) and subtraction (Figs. 9b and c) of the electric signals measured before the notch when the A_0 and S_0 modes are launched, respectively and encounter a 3 mm deep asymmetric notch (p=3/6). Its shown that the application of the addition and subtraction operations allow to separate the anti-symmetrical contribution from the symmetrical one. On these figures, the incident (in), the first reflection (re_1) of the non-converted and the converted modes are identified and quantified. Furthermore, multiple reflections from the edges of the notch and the plate are also observed.

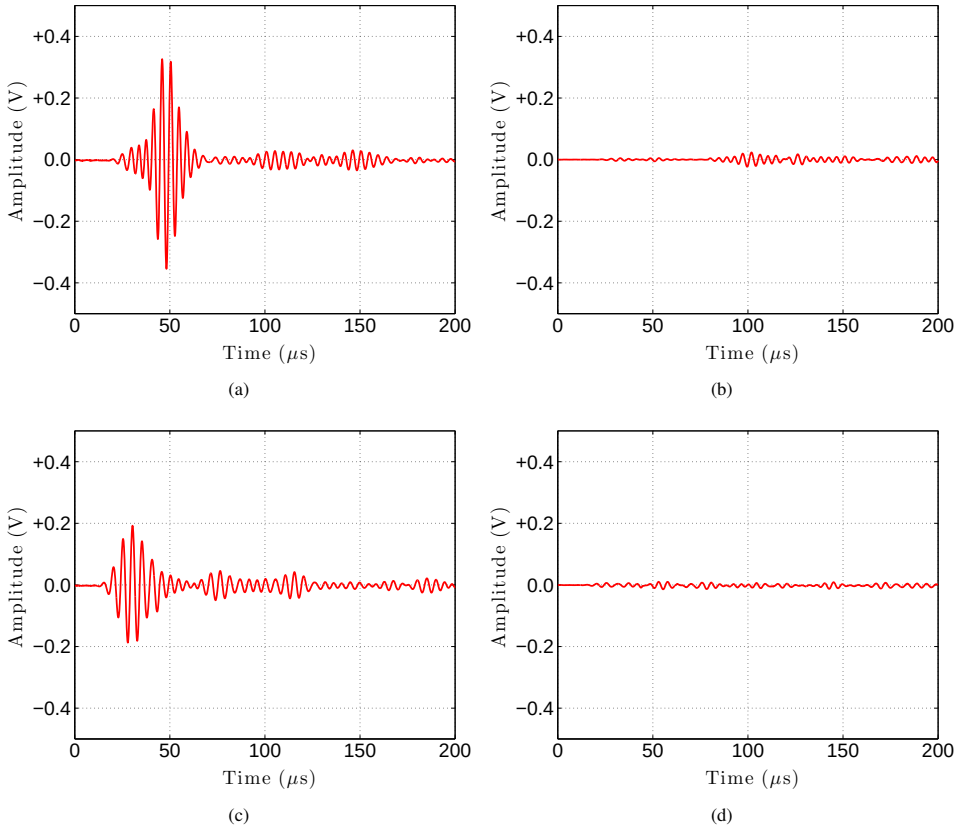

Figure 9. Mean results before the notch of 3 mm deep at a distance of 185 mm from the left of the plate edge: (a) addition and (b) subtraction when the A_0 mode is lunched, (c) subtraction and (d) addition when the S_0 mode is lunched.

4.2. Determination of the power coefficients

The determination of the power coefficients from only the temporal normal or tangential displacement at a given location on the plate surface was presented in previous works [13–15]. Hence, the power reflection and transmission coefficients of the n^{th} Lamb mode when the n^{th} mode is driven for the symmetric or asymmetric step-down damage are:

$$R_{nn}^{Nor} = \left| \frac{\widetilde{W}_{n(re)}(x_1, d)}{\widetilde{W}_{n(in)}(x_1, d)} \right|^2 , \tag{1}$$

and

$$T_{nn}^{Nor} = \left| \frac{\widetilde{W}_{n(tr)}(x_1, dp)}{\widetilde{W}_{n(in)}(x_1, d)} \right|^2 \left| \frac{\widetilde{W}^0_{n(in)}(d)}{\widetilde{W}^0_{n(tr)}(dp)} \right|^2 \frac{\widetilde{P}_{nn}|_{2dp}}{\widetilde{P}_{nn}|_{2d}} , \tag{2}$$

where the first subscript (n) of R and T designates the incident Lamb mode and the second one (n) designates the reflected or the transmitted mode. $\widetilde{W}^0_n$ corresponds to the modal (eigen value) normal harmonic displacement and $\widetilde{W}_n$ corresponds to the normal displacement. The tilde symbol ($\widetilde{\ }$) indicates that the corresponding quantity is calculated at the central frequency. The superscript Nor indicates that the normal displacement is used to compute the above coefficients. in, re and tr denote the terms incident, reflected and transmitted, respectively. x_1 is the propagation direction. P_{nn} is the average power flow of the n^{th} Lamb mode at the central frequency [29]. The notations $|_{2d}$ and $|_{2dp}$ indicate that the average power flow is calculated for a plate thickness of $2d$ and $2dp$, respectively.

Moreover, the asymmetrical discontinuities produce a converted fundamental Lamb mode noted m. Therefore, the power reflection and transmission coefficients of the m^{th} Lamb mode when the n^{th} mode is driven for an asymmetric step-down damage are computed as:

$$R_{nm}^{Nor} = \left| \frac{\widetilde{W}_{m(re)}(x_1, d)}{\widetilde{W}_{n(in)}(x_1, d)} \right|^2 \left| \frac{\widetilde{W}^0_{n(in)}(d)}{\widetilde{W}^0_{m(re)}(d)} \right|^2 \frac{\widetilde{P}_{mm}|_{2d}}{\widetilde{P}_{nn}|_{2d}} , \tag{3}$$

and

$$T_{nm}^{Nor} = \left| \frac{\widetilde{W}_{m(tr)}(x_1, dp)}{\widetilde{W}_{n(in)}(x_1, d)} \right|^2 \left| \frac{\widetilde{W}^0_{n(in)}(d)}{\widetilde{W}^0_{m(tr)}(dp)} \right|^2 \frac{\widetilde{P}_{mm}|_{2dp}}{\widetilde{P}_{nn}|_{2d}} . \tag{4}$$

Instead of the normal displacement, the tangential one could be also used to compute these coefficients. Then, the corresponding values are noted R_{nn}^{Tan}, T_{nn}^{Tan}, R_{nm}^{Tan} and T_{nm}^{Tan}.

In fact, $\widetilde{W}^0_n$ and $\widetilde{W}^0_m$ are determined analytically while, $\widetilde{W}_n$ and $\widetilde{W}_m$ are measured experimentally or computed numerically. When studies are carried out in transient regime, the measured or computed displacements are taken at the central working frequency, which corresponds to the maximum of the Lamb wave packet envelope.

4.3. Numerical computations

4.3.1. General description of the simulation

A lossless aluminium plate is considered with thickness ($2d$) and length ($2L$) equal to 6 mm and 500 mm, respectively. The longitudinal velocity (c_L), the transverse velocity (c_T) and the density (ρ) of this plate are equal to 6422 m/s, 3110 m/s and 2695 kg/m^3, respectively. Figs. 10a and 12a illustrate a

http://dx.doi.org/10.5772/54582

plate containing a meshed symmetrical and asymmetrical notches, respectively. Here, notches have a variable width equal to w. The meshing of the symmetrical and asymmetrical steps down are illustrated on Figs. 10b and 12b, respectively. The meshing of the symmetrical and asymmetrical steps up are illustrated on Figs. 10c and 12c, respectively. In all steps, the plate thickness changes abruptly either from $2d$ to $2dp$ or from $2dp$ to $2d$. d is the half thickness of the plate and p takes values from 0 to 1 with a constant increment. In this work, more than 10 isoparametric eight-node quadrilateral elements are used for one wavelength to maintain a large accuracy of the Finite Element (FE) results.

In this paper, the fundamental Lamb mode, A_0 or S_0, is launched from the edge of the plate by the application of the appropriate displacement shapes. The excitation signals (e_n) are windowed by a Hanning temporal function and the central working frequency is f_c=200 kHz. The tone burst number is N_{cyc}=10 and the time sampling period is Δt=0.1 μs.

4.3.2. Symmetrical notches

Figure 11 shows a comparison between the reflection and transmission coefficients for the symmetrical step down and step up. These coefficients are obtained by launching either the A_0 mode (Fig. 11a) or the S_0 mode (Fig. 11b). From the results of Fig. 11, relations of equality can be observed and expressed by the following equations:

$$R_n^D = R_n^I \,, \tag{5}$$

$$T_n^D = T_n^I \,, \tag{6}$$

where D and I designate Direct and Inverse for step down and step up damage, respectively.

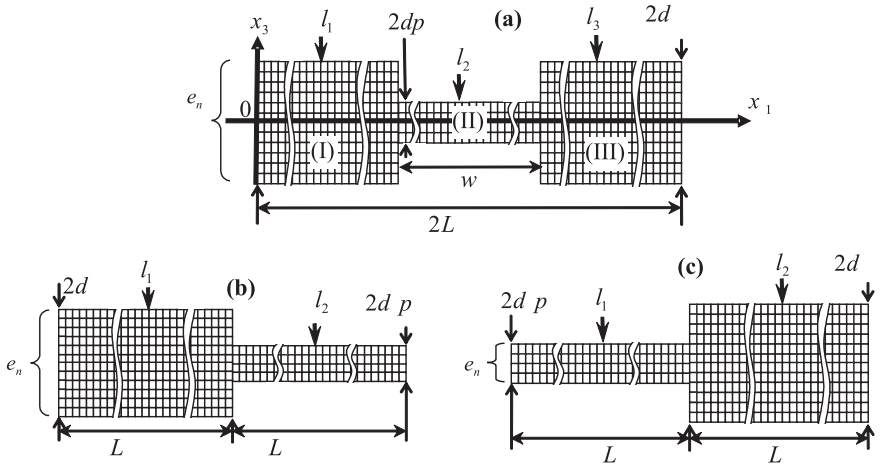

Figure 10. Mesh of an aluminium plate with a symmetrical notch (a), a symmetrical step down (b) and a symmetrical step up (c).

As said in the introduction, the above equations are valid if the frequency of the selected fundamental Lamb modes are taken under the cut-off frequencies of A_1 and S_1 modes. The observed small errors on Figs. 11a and b are due to the mesh precision of the FE meshing at the left edge of the plate. Indeed, the applied excitation in the symmetrical step up case is performed on fewer nodes along the thickness than for the symmetrical step down case.

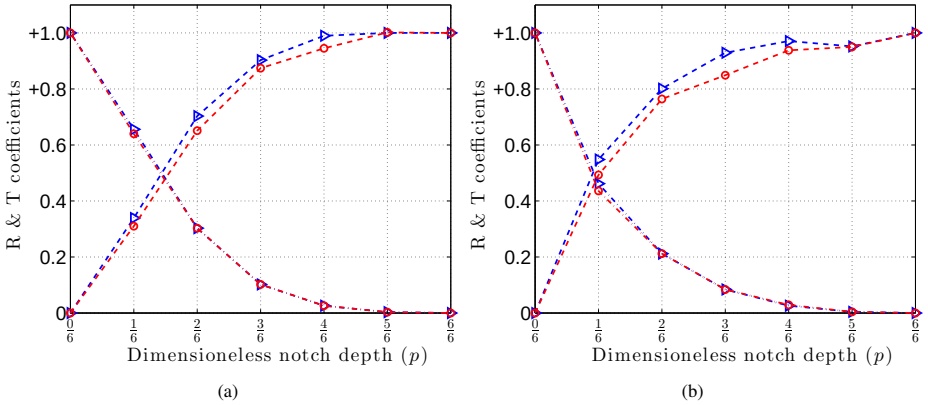

Figure 11. Comparison between the reflection (—·) and transmission (— —) power coefficients computed at 200 kHz for a symmetric step down (▷) and step up (○) when the A_0 (a) and S_0 (b) modes are launched.

The symmetrical notch is now decomposed as the superposition of a symmetrical step down and step up as shown on Fig. 10. The incident power I performed on the symmetrical step down is equal to unity, while the incident power transmitted to the symmetrical step up becomes equal to T_1. Using these remarks and the equality relation between the symmetrical step down and step up (Eqs. (5) and (6)), it is easy to obtain the following relationship:

$$\frac{R_2}{R_1} = \frac{T_1}{I} = T_1 \, . \tag{7}$$

Indeed, this relation shows that the reflected power compared to the incident power is equivalent for the symmetrical step down and step up. Furthermore, using the power balance at the interface of the regions (I) and (II), i.e. $R_1 + T_1 = 1$, and at the interface of the regions (II) and (III), i.e. $R_2 + T_2 = T_1$, R_2 and T_2 can be simply expressed as: $R_2 = R_1(1 - R_1)$ and $T_2 = (1 - R_1)^2$. Consequently, these relations show that with one FE simulation of the symmetrical step down or the symmetrical step up, all coefficients (R_1, R_2, T_1 and T_2) of the symmetrical notch can be derived.

4.3.3. Asymmetrical notches

Figures 13 and 14 show a comparison between the power coefficients for the asymmetrical step down and step up when the driven mode is the A_0 and the S_0 mode, respectively. Figures. 13a and 14a illustrate the reflection coefficients and Figures. 13b and 14b depict the transmission coefficients. On Figs. 13, a significant reflection of the driven mode A_0 and a low mode conversion from the A_0 to the S_0 mode are observed for the asymmetrical step up. On the contrary, a significant mode conversion

http://dx.doi.org/10.5772/54582

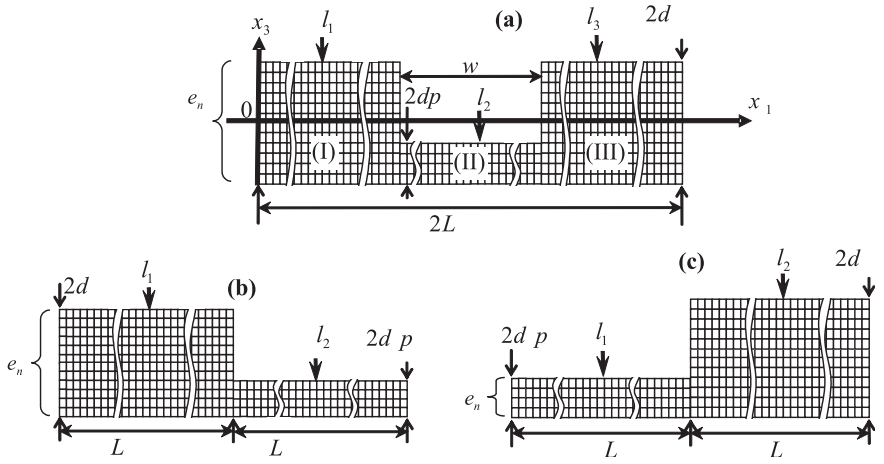

Figure 12. Mesh of an aluminium plate with an asymmetrical notch (a), an asymmetrical step down (b) and an asymmetrical step up (c).

from the S_0 to the A_0 mode for the transmission region is shown on Figs. 14. Therefore, the A_0 mode is more sensitive to the asymmetrical step up than the S_0 mode on the basis of the power reflection. However, the S_0 mode is more sensitive to the asymmetrical step up than the A_0 mode on the basis of the power conversion. The behaviour of the A_0 and S_0 modes towards the asymmetrical step down and step up seems to be inverted.

It is worth mentioning that a simple relation can be observed and expressed when the n^{th} Lamb mode is driven as $R^D_{nm} \cong R^I_{nm}$ and $T^D_{nn} \cong T^I_{nn}$. The observed small errors on Figs. 13 and 14 are due to the mesh precision of the FE meshing at the left edge of the plate as mentioned in the symmetrical case.

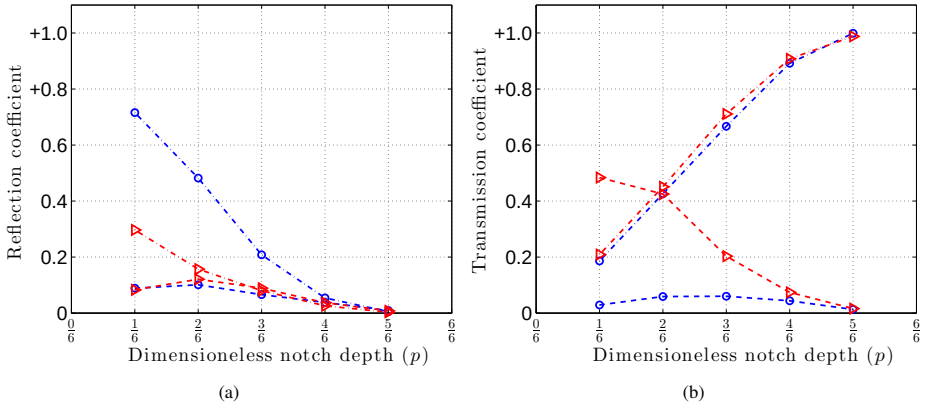

Figure 13. Comparison between the power reflection (a) and the transmission (b) coefficients of the A_0 (—·) and S_0 (— —) modes computed for an asymmetric step down (▷) and step up (○) when the A_0 mode is launched.

In this section, the asymmetrical notch is studied as a superposition of the asymmetrical step down and step up as shown on Fig. 12. The incident power I_n performed on the asymmetrical step down is equal

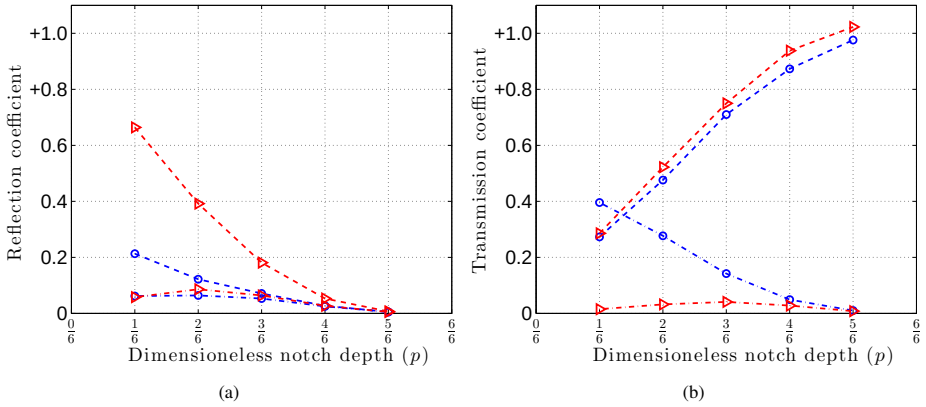

Figure 14. Comparison between the power reflection (a) and the transmission (b) coefficients of the A_0 (—·) and S_0 (——) modes computed for an asymmetric step down (▷) and step up (○) when the S_0 mode is launched.

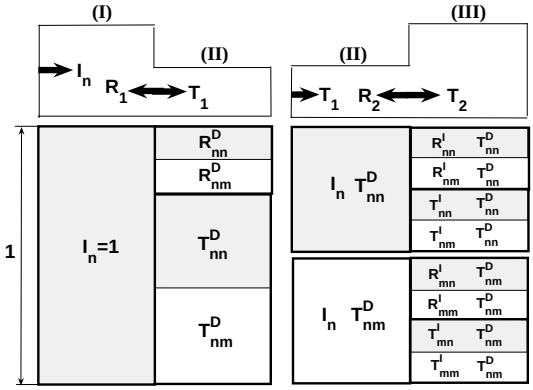

Figure 15. Schematic power balance of the combination of an asymmetric step down and step up.

to unity, while the incident power for the asymmetrical step up becomes equal to $T_{nn}^D + T_{nm}^D$ which corresponds to $T_{1,nn} + T_{1,nm}$ (Fig. 15). Hence, each transmitted wave packet produces four new wave packets. Therefore, the power balance can be expressed for an asymmetrical step up as:

$$(R_{nn}^I + R_{nm}^I + T_{nn}^I + T_{nm}^I)T_{nn}^D = T_{nn}^D\,, \tag{8}$$

$$(R_{mn}^I + R_{mm}^I + T_{mn}^I + T_{mm}^I)T_{nm}^D = T_{nm}^D\,, \tag{9}$$

Then, the power balance of a constructed asymmetrical notch is derived [14] as:

$$R_{nn}^D + R_{nm}^D + (R_{nn}^I + R_{nm}^I + T_{nn}^I + T_{nm}^I)T_{nn}^D + (R_{mn}^I + R_{mm}^I + T_{mn}^I + T_{mm}^I)T_{nm}^D = 1. \tag{10}$$

http://dx.doi.org/10.5772/54582

Indeed, all the coefficients of the asymmetrical notch can be derived by analogy from the asymmetrical step down and step up results when the fundamental Lamb mode A_0 or S_0 is launched. Hence, all the coefficients of the complete asymmetrical notch can be computed as for example: $R_{2,mn} = R^I_{mn}\, T^D_{nm}$, $T_{2,mn} = T^I_{mn}\, T^D_{nm}$, $R_{2,mm} = R^I_{mm}\, T^D_{nm}$ and $T_{2,mm} = T^I_{mm}\, T^D_{nm}$.

Furthermore, all the multiple reflections and transmissions and mode conversions of the FEM can now be identified and quantified. This construction method can be generalised to study the interaction of the fundamental Lamb modes with several discontinuities only by using the asymmetrical step down and step up results.

However, the construction technique is valuable only for the fundamental Lamb modes taken under their cut-off frequencies and the notch width verifying:

$$w > w_{lim} = \frac{1}{4} N_{cyc}\, \mathtt{min}(\lambda_{A_0}, \lambda_{S_0})\ , \tag{11}$$

where `min` designates minimum. If the rectangle window is used instead of the Hanning one, this limit is given by $\frac{1}{2} N_{cyc}\ \lambda$. In the case of the symmetrical notch, the notch width must verify $w > w_{lim} = \frac{1}{4} N_{cyc}\ \lambda_{(A_0 \text{ or } S_0)}$ when the A_0 or S_0 mode is launched.

4.4. Comparisons and validation

Figures. 16a and b show power coefficient comparisons between numerical and experimental results of the interaction of the A_0 and S_0 modes, respectively with different depths of symmetrical notches. Several experimental measurements (20) are performed to determine the displayed error bars. Good agreement is found for both the A_0 and S_0 cases.

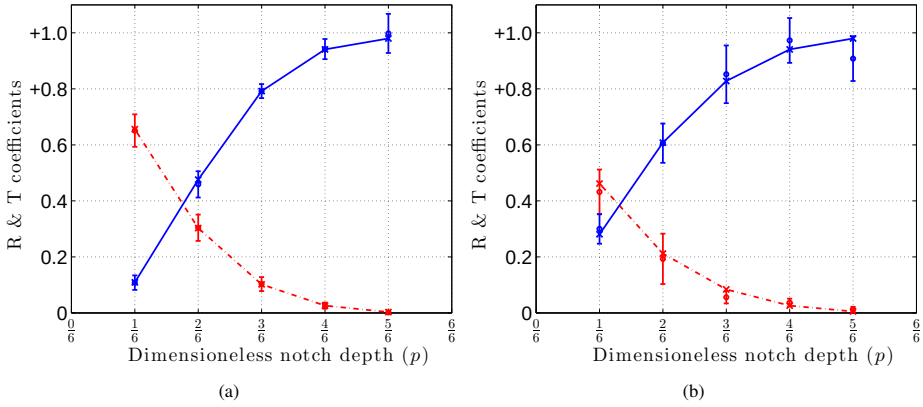

Figure 16. Comparison between numerical and experimental results of the power reflection (—·) and transmission (—) coefficients of the modes A_0 (a) and S_0 (b) when they are launched and interact with symmetrical notches.

Figures 17a and b show power reflection coefficient comparisons between numerical and experimental results of the interaction of the A_0 and S_0 modes, respectively with different depths of asymmetrical notches. Here again, good agreement is found for both the A_0 and S_0 driven modes.

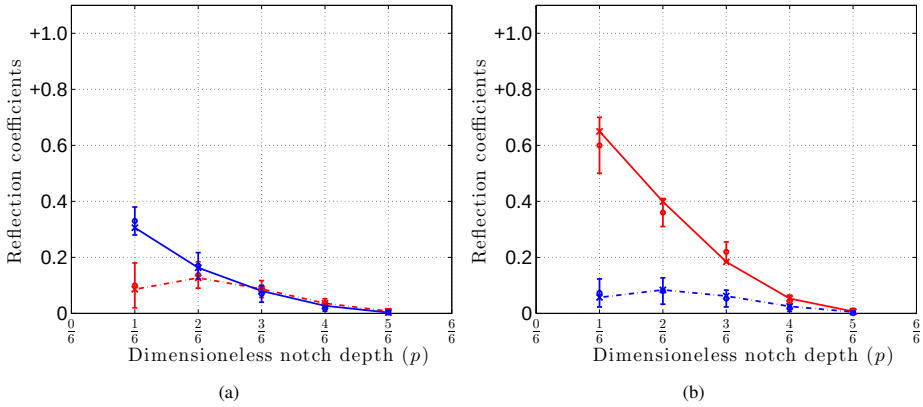

Figure 17. Comparison between numerical and experimental results of the power reflection coefficients of the A_0 (—) and S_0 (– –) modes when the A_0 (a) or S_0 (b) mode is launched and interacts with asymmetrical notches.

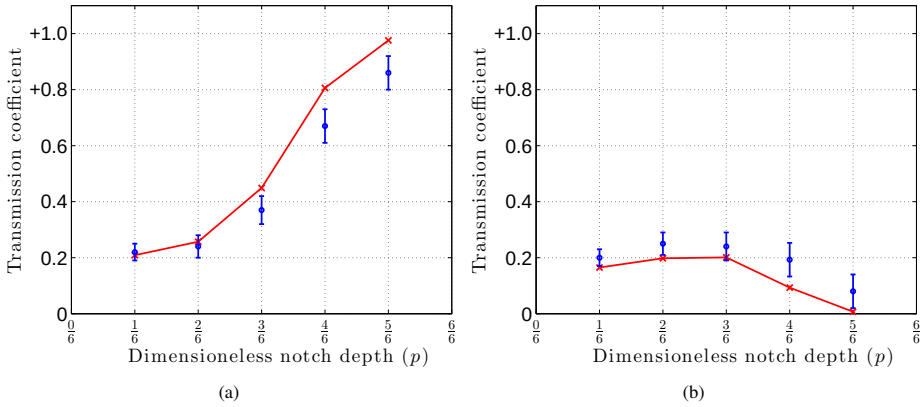

Figure 18. Comparison between numerical (—) and experimental (•) results of the power transmission coefficients of the A_0 (a) and S_0 (b) modes when the A_0 mode is launched and interacts with asymmetrical notches.

The numerical results [14] have shown that the study of the transmission region is very difficult and requires a careful analysis. The power transmission coefficients when the A_0 mode is launched are depicted on Figures 18a and b and show an agreement with the numerical results. However, when the S_0 mode is launched, errors due to the experimental conditions do not permit the obtaining of a sufficient precision to separate and quantify the existent Lamb modes in this region. In fact, the high velocity of the S_0 mode increases the interferences between reflections from the start and the end of the notch edges.

5. Conclusion

Transducers piezoceramic based emitter is developed to excite one selected Lamb mode. To this end, two piezoelectric transducers are cut and placed on the opposite sides of the tested plate. Then

http://dx.doi.org/10.5772/54582

the in-phased and in-anti-phased electrical signals are applied to select the A_0 or the S_0 mode. Noteworthy that a calibration process is carried to avoid the receiver effects for the reflection study. The power refection and transmission coefficients are then obtained by using either experimental measurements or numerical predictions and normal mode expansions. This has the advantage to allow a direct comparison between numerical and experimental results. Symmetrical and asymmetrical discontinuities are both investigated. The construction of power coefficients of symmetrical notches from those obtained for one elementary configuration is carried out successfully. Furthermore, the power coefficients for asymmetrical notches are constructed from those obtained for two elementary configurations (step down and step up). On the contrary of the symmetrical discontinuities, the asymmetrical ones enable mode conversions. The experimental measurements are confronted with success to numerical predictions.

Author details

Farouk Benmeddour[1,⋆], Emmanuel Moulin[1],
Jamal Assaad[1] and Sonia Djili[2]

1 IEMN, OAE Department, CNRS UMR 8520, University of Valenciennes and Hainaut Cambrésis, Le Mont Houy 59313 Valenciennes Cedex 9, France
2 Scientific and Technical Center of Research on Welding and Control, BP 64, route de Daly Brahim. Chéraga, 16000 Algies, Algeria

References

[1] Lamb H. On waves in an elastic plate. Proc Roy Soc London. 1917;A 93:114–128.

[2] Diligent O, Grahn T, Boström A, Cawley P, Lowe MJS. The low-frequency reflection and scattering of the S0 Lamb mode from a circular through-thickness hole in a plate: Finite Element, analytical and experimental studies. J Acoust Soc America. 2002;112 (6):2589–2601.

[3] Hayashi T, Kawashima K. Single mode extraction from multiple modes of Lamb wave and its application to defect detection. JSME Int J. 2003;46 (4):620–626.

[4] Castaings M, Le Clézio E, Hosten B. Modal decomposition method for modeling the interaction of Lamb waves with cracks. J Acoust Soc America. 2002;112 (6):2567–2582.

[5] Wang L, Shen J. Scattering of elastic waves by a crack in a isotropic plate. Ultrasonics. 1997;35:451–457.

[6] Cho Y, Rose JL. An elastodynamic hybrid boundary element study for elastic wave interactions with a surface breaking defect. International Journal of Solids and Structures. 2000;37:4103–4124.

[7] Hansch MKT, Rajana KM, Rose JL. Characterization of aircraft joints using ultrasonic guided waves and physically bases feature extraction. IEEE Ultrasonics Symposium. 1994;p. 1193–1196.

[8] Cho Y. Estimation of Ultrasonic guided wave mode conversion in a plate with thickness variation. IEEE Trans Ultrason Ferroelectr Freq Control. 2000;17 (3):591–603.

[9] Leduc D, Hladky AC, Morvan B, Izbicki JL, Pareige P. Propagation of Lamb waves in a plate with periodic grating: Interpretation by phonon. J Acoust Soc America. 2005;118 (4):2234–2239.

[10] Alleyne DN, Cawley P. A 2-dimensional Fourier transform method for the quantitative measurement of Lamb modes. IEEE Ultrasonics Symposium. 1990;p. 1143–1146.

[11] Lowe MJS, Diligent O. Low-frequency reflection characteristics of the S0 Lamb wave from a rectangular notch in a plate. J Acoust Soc America. 2002;111(1):64–74.

[12] Jin J, Quek ST, Wang Q. Wave boundary element to study Lamb wave propagation in plates. J Sound and Vibration. 2005;288:195–213.

[13] Benmeddour F, Grondel S, Assaad J, Moulin E. Study of the fundamental Lamb modes interaction with symmetrical notches. NDT & E International. 2008;41(1):1–9.

[14] Benmeddour F, Grondel S, Assaad J, Moulin E. Study of the fundamental Lamb modes interaction with asymmetrical discontinuities. NDT & E International. 2008;41(5):330–340.

[15] Benmeddour F, Grondel S, Assaad J, Moulin E. Experimental study of the A0 and S0 Lamb waves interaction with symmetrical notches. Ultrasonics. 2009;49(2):202 – 205.

[16] El Youbi F, Grondel S, Assaad J. Signal processing for damage detection using two different array transducers. Ultrasonics. 2004;42:803–806.

[17] Si-Chaib MO, Djelouah H, Bocquet M. Applications of ultrasonic reflection mode conversion transducers in NDE. NDT & E International. 2000;33(2):91 – 99.

[18] Duquennoy M, Ouaftouh M, Qian ML, Jenot F, Ourak M. Ultrasonic characterization of residual stresses in steel rods using a laser line source and piezoelectric transducers. NDT & E International. 2001;34(5):355 – 362.

[19] Yan T, Theobald P, Jones BE. A self-calibrating piezoelectric transducer with integral sensor for in situ energy calibration of acoustic emission. NDT & E International. 2002;35(7):459 – 464.

[20] Blomme E, Bulcaen D, Declercq F. Air-coupled ultrasonic NDE: experiments in the frequency range 750kH-2MHz. NDT & E International. 2002;35(7):417 – 426.

[21] Martínez O, Akhnak M, Ullate LG, de Espinosa FM. A small 2D ultrasonic array for NDT applications. NDT & E International. 2003;36(1):57 – 63.

[22] Bhalla S, Soh CK. High frequency piezoelectric signatures for diagnosis of seismic/blast induced structural damages. NDT & E International. 2004;37(1):23 – 33.

[23] Sun M, Staszewski WJ, Swamy RN, Li Z. Application of low-profile piezoceramic transducers for health monitoring of concrete structures. NDT & E International. 2008;41(8):589 – 595.

[24] Rathod VT, Mahapatra DR. Ultrasonic Lamb wave based monitoring of corrosion type of damage in plate using a circular array of piezoelectric transducers. NDT & E International. 2011;44(7):628 – 636.

http://dx.doi.org/10.5772/54582

[25] Chung CH, Lee YC. Fabrication of poly(vinylidene fluoride-trifluoroethylene) ultrasound focusing transducers and measurements of elastic constants of thin plates. NDT & E International. 2010;43(2):96 – 105.

[26] Ribichini R, Cegla F, Nagy PB, Cawley P. Experimental and numerical evaluation of electromagnetic acoustic transducer performance on steel materials. NDT & E International. 2012;45(1):32 – 38.

[27] Lee YC, Lin Z. Miniature piezoelectric conical transducer: Fabrication, evaluation and application. Ultrasonics. 2006;44, Supplement:e693 – e697. Proceedings of Ultrasonics International (UI) and World Congress on Ultrasonics (WCU).

[28] Bowen CR, Bradley LR, Almond DP, Wilcox PD. Flexible piezoelectric transducer for ultrasonic inspection of non-planar components. Ultrasonics. 2008;48(5):367 – 375.

[29] Auld BA. Acoustic fields and waves in solids. vol. II. A Wiley-Interscience publication; 1973.